Control of Single-Phase Grid-Connected Converters With *LCL* Filters Using Recurrent Neural Network and Conventional Control Methods

Xingang Fu, *Student Member, IEEE*, and Shuhui Li, *Senior Member, IEEE*

***Abstract*—Single-phase grid-connected inverters are widely used to connect small-scale distributed renewable resources to the grid. However, unlike a three-phase system, control for a single-phase inverter is more challenging, especially when the inverter is used with an *LCL* filter. This paper proposes a novel recurrent neural network-based vector control method for a single-phase inverter with an *LCL* filter. The neural network is trained based on adaptive dynamic programming principle, and the objective of the training is to approximate optimal control. The Levenberg–Marquardt plus forward accumulation through time algorithm is developed for training the proposed recurrent neural network controller. The neural network vector control approach is compared with the conventional control methods, including the conventional PI-based vector control method and the PR-based control technique for single-phase inverters. Both the simulations and hardware experiments demonstrate the great advantages of the proposed neural network vector control over the conventional control methods. Compared with conventional control methods, the neural network control allows for low sampling rate and low switching frequency, while maintaining high performance in controlling a single-phase inverter. In addition, no specific damping policy is required to implement the proposed neural network vector control for an *LCL*-filter based single-phase inverter. The study shows that the neural network vector control is a robust control method, and can provide better control performance even when facing system parameter changes, while under this case, both the conventional PI-based vector control and the PR-based control failed to yield the acceptable results.**

***Index Terms*—Approximate optimal control, forward accumulation through time, *LCL* filter, Levenberg–Marquardt, proportional resonant control, recurrent neural networks, single-phase inverter, vector control.**

I. Introduction

SINGLE-PHASE grid-connected inverters are playing an increasingly important role as the interface between renewable energy sources and the utility grid [1]–[4], especially in small scale photovoltaic applications. In existing technologies, the primary technologies for control of a single-phase inverter include PI-based vector control approach and PR-based control method. The PI-based vector control approach has been widely used to control three-phase grid-connected inverters [5], [6], due to its great advantages. However, to apply vector control to a single-phase grid-connected inverter, an imaginary circuit needs to be created. Many researchers have investigated on how to create the imaginary circuit. Zhang *et al.* [7] proposed to delay the real circuit variables by a quarter cycle of the fundamental period. However, disadvantage of this method is that it would cause a delay of the system, thereby deteriorating the dynamic response of the system. Roshan *et al.* [8] used differentiation to create the imaginary circuit to avoid the delay. But, the performance of the differentiation approach can be deteriorated significantly under distorted grid voltage conditions. Bahrani *et al.* [9] developed a fictive-axis emulation technique to create the imaginary circuit with a fictive axis running concurrently with the real circuit, which helps improve the poor dynamics of the conventional approaches.

The conventional PI-based vector control for a single-phase *LCL* filter-based grid-connected converter (GCC) is equivalent to that for a three-phase *LCL*-based GCC by neglecting the capacitor. This kind of simplification would result in an imprecise description of an *LCL* inverter system and potential oscillatory and/or unstable dynamic behavior if the *LCL* filter or the controller is not properly damped [6], [10]. Passive damping methods (see [11]) cause a decrease of the overall system efficiency because of the associated power losses, while Active damping (AD) methods (see [12], [13]) are more selective to parameter uncertainties [14].

For a single-phase GCC, it would be much more challenging to implement the vector control due the imaginary circuit issue. As a result, lots of research has been done on the proportional resonant (PR) control (see [3], [15], [16]) for single phase GCCs, which does not need to create the imaginary circuit and the controller is based on PR controller instead of PI controller. However, this kind of control strategy generally requires very high sampling frequency (e.g., 15 kHz) and switching frequency (e.g., 15 kHz) in [3]. In general, high switching frequency tends to cause more energy loss.

In recent years, significant research has been conducted in the area of dynamic programming (DP) [17] for optimal control of nonlinear systems [18]. Adaptive critic designs constitute a class of approximate dynamic programming (ADP) methods that use the incremental optimization techniques combined with parametric structures to approximate the optimal cost and control of a system [19], [20]. In [21], both heuristic dynamic

Manuscript received May 8, 2015; revised August 18, 2015; accepted October 2, 2015. Date of publication October 13, 2015; date of current version January 28, 2016. This work was supported in part by the U.S. National Science Foundation under Grant EECS 1102038/1414379. Recommended for publication by Associate Editor K.-B. Lee.

The authors are with the Department of Electrical and Computer Engineering, The University of Alabama, Tuscaloosa, AL 35487 USA (e-mail: xfu@crimson.ua.edu; sli@eng.ua.eduu).

Color versions of one or more of the figures in this paper are available online at http://ieeexplore.ieee.org.

Digital Object Identifier 10.1109/TPEL.2015.2490200

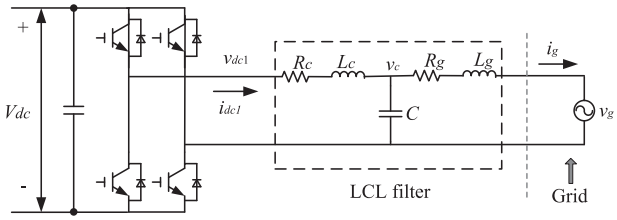

Fig. 1. Schematic of a single-phase *LCL*-GCC.

programming and dual heuristic programming have been used to control a turbogenerator. In [22], an ADP-based neural network (NN) controller is trained and used to control a three-phase *L*-filter-based GCC system [22], [23], which demonstrated an excellent performance compared to a conventional vector controller.

However, no research has been conducted on vector control of a single-phase *LCL*-filter-based inverter using an ADP-based neural network. The purpose of this paper is to investigate a NN vector control method for the optimal vector control of a single-phase LCL-filter-based inverter, and compare it with conventional PI-based vector control and PR-based control methods. The special features and contributions of the paper include: 1) An approach to implement optimal vector control for the single-phase *LCL*-GCC by using an artificial NN, 2) a mechanism to train the NN controller by using a novel Levenberg–Marquardt (LM) + Forward Accumulation Through Time (FATT) algorithm, 3) investigation and comparison of the NN vector controller with the conventional vector controller and the PR controller, and 4) hardware experiment implementation, validation, and comparison.

The rest of the paper is structured as follows. The conventional PI based vector control and PR based control methods for a single-phase LCL-filter-based inverter system are presented in Section II. Section III explains the proposed NN vector control topology for a single-phase LCL-filter-based inverter. How to train the NN vector controller is discussed in Section IV. Section V investigates the performance of the NN controller, and compares it with the conventional controllers in power converter switching environment. Section VI presents hardware experiment validation and comparison of the NN vector control, the conventional vector control and the PR control. Finally, the paper concludes with summary remarks in Section VII.

II. Single Phase *LCL*-GCC and Its Conventional Control Approaches

A. Single Phase LCL-GCC

Fig. 1 shows the schematic of a single-phase *LCL*-GCC, in which a dc-link capacitor is on the left, an *LCL* filter is placed in the middle, and a single-phase voltage source, representing the voltage at the point of common coupling (PCC) of the ac system, is on the right [2], [3].

Using the motor sign convention (i.e., the power flowing into the GCC as positive), the voltage balance across the grid-side inductor, the voltage balance across the inverter-side inductor, and the current balance across the *LCL* capacitor can be expressed as

$$\begin{cases} v_g = R_g i_g + L_g \dfrac{di_g}{dt} + v_c \\ v_c = R_c i_{\rm dc1} + L_c \dfrac{di_{\rm dc1}}{dt} + v_{\rm dc1} \\ i_g = i_{\rm dc1} + C \dfrac{dv_c}{dt} \end{cases} \tag{1}$$

where R_g, L_g, R_c, L_c, C, v_g, v_c, $v_{\rm dc1}$, i_g, and $i_{\rm dc1}$ represent the grid-side resistor, the grid-side inductor, the converter-side resistor, the converter-side inductor, the parallel capacitor, the grid voltage, the capacitor voltage, the converter voltage, the grid current, and the converter-side current, respectively.

B. Proportional Resonant Control

The configuration of the typical PR Control for a single-phase inverter consists of an outer-loop controller and an inner current loop controller. The outer-loop controller utilizes the PI controller to control the dc-link voltage or PCC active power and PCC reactive power, respectively. To achieve this, the PCC current, $i_g(t) = I_m \cos(\omega t - \phi)$ (I_m stands for the amplitude of $i_g(t)$), is normally expressed as one in-phase current component $i_P(t)$ plus one out-of-phase current component $i_Q(t)$ as

$$i_p(t) = \underbrace{I_m \cos(\phi)}_{I_P} \cos(\omega t), \quad i_p(t) = \underbrace{I_m \sin(\phi)}_{I_Q} \sin(\omega t) \tag{2}$$

Then, the control of PCC active and reactive power can be achieved through the control of $i_P(t)$ and $i_Q(t)$ [24] or I_P and I_Q, respectively.

The inner current loop controller assures that the reference current $i_{g\_\rm ref}(t) = I_{P\_\rm ref} \cos(t) + I_{Q\_\rm ref} \sin(t)$ generated by the outer-loop controller is followed through a PR controller. For the effective tracking of instantaneous reference current waveform $i_{g\_\rm ref}(t)$, a fast switching frequency is usually needed for the PR-controlled GCC [3], which would increase the loss of the converter. Another challenge associated with the PR controlled GCC is that the control of $i_g(t)$ at the PCC has to be achieved indirectly through the control of $i_{\rm dc1}(t)$, which would affect the effectiveness of the active and reactive power control at the PCC.

Fig. 2 depicts the standard PR control configuration for a single-phase *LCL*-GCC. The current error e_i is supplied to the parallel connection of a PR controller and a harmonic compensator. Note that the inverter current $i_{\rm dc1}$ is measured instead of the grid current [3], [15], [16].

The Laplace transform of the PR controller is

$$G_{\rm PR}(s) = K_p + \frac{2K_r s}{s^2 + \omega_s^2}, \quad \omega_s = 2\pi f_s \tag{3}$$

where K_p is the proportional gain, and K_r is the gain for the generalized integrator $\frac{2s}{s^2+\omega_o^2}$, which is also a bandpass filter tuned to resonate at the grid frequency f_s. The harmonic compensator is formed by several bandpass filters (4) which are

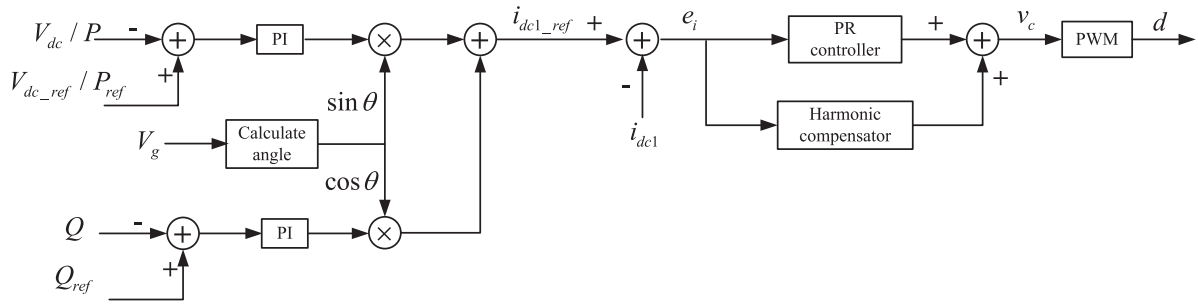

Fig. 2. Standard PR control configuration for a single-phase *LCL*-GCC.

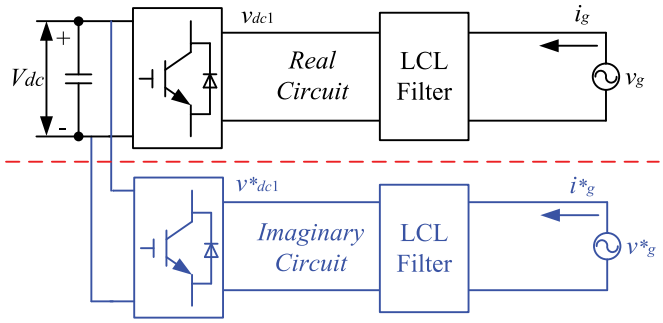

Fig. 3. Creating the imaginary circuit based on real circuit of the single-phase *LCL*-GCC.

tuned to resonate at the desired harmonic frequency $n\omega_o$

$$H_c(s) = \sum_{n=3}^{h} \frac{K_n s}{s^2 + (n\omega_s)^2} \tag{4}$$

where $n = 3, 4, \ldots, h$ and h is the highest current harmonic component to be attenuated.

C. Decoupled Vector Control

The conventional decoupled vector control method for a single-phase *LCL*-GCC is similar to that for a three-phase *LCL*-GCC [7]. The only difference is that an imaginary orthogonal circuit needs to be created based on the real circuit to implement the vector control.

The current and voltage variables in the imaginary circuit should have exactly the same amplitude as those in the the real circuit (shown as Fig. 3) but $\pi/2$ phase shift. Thus, corresponding to the α-axis (1), the imaginary or β-axis voltage and current equations are

$$\begin{cases} v_g^* = R_g i_g^* + L_g \dfrac{di_g^*}{dt} + v_c^* \\ v_c^* = R_c i_{\mathrm{dc1}}^* + L_c \dfrac{di_{\mathrm{dc1}}^*}{dt} + v_{\mathrm{dc1}}^* \\ i_g^* = i_{\mathrm{dc1}}^* + C \dfrac{dv_c^*}{dt} \end{cases} \tag{5}$$

where, v_g^*, v_c^*, v_{dc1}^*, i_g^*, and i_{dc1}^* stand for the grid voltage, the capacitor voltage, the converter voltage, the grid current, and the converter-side current in the imaginary circuit, respectively. Further, $v_g^* = v_g e^{-\pi/2}$, $i_g^* = i_g e^{-\pi/2}$, etc. The real and imaginary circuits together constitute the α-β frame of the *LCL*-GCC system, which can be transferred into the d-q frame using the transformation matrix T (6) [7]. Also, the inverse transformation matrix from d-q frame to α-β frame is just inverse of matrix T [7]

$$T = \begin{bmatrix} \cos(\omega t) & \sin(\omega t) \\ -\sin(\omega t) & \cos(\omega t) \end{bmatrix} \tag{6}$$

Omitting the capacitance impact [5], the vector control for *LCL*-GCCs takes exactly the same policy as that for *L*-GCCs. Thus in the α-β frame, the single-phase *LCL*-GCC (1) and (5) are simplified into

$$\begin{cases} v_g = (R_c + R_g) i_g + (L_c + L_g) \dfrac{di_g}{dt} + v_{\mathrm{dc1}} \\ v_g^* = (R_c + R_g) i_g^* + (L_c + L_g) \dfrac{di_g^*}{dt} + v_{\mathrm{dc1}}^* \end{cases} \tag{7}$$

Further, after applying the transformation matrix T to (7), (8) gives the equations in d-q frame that are used to design current control loop of the simplified single-phase *LCL*-GCCs

$$\begin{cases} v_{d1} = -\underbrace{\left[(R_c + R_g) i_d + (L_c + L_g) \dfrac{di_d}{dt} \right]}_{v_d'} + \omega_s (L_c + L_g) i_q + v_d \\ v_{q1} = -\underbrace{\left[(R_c + R_g) i_q + (L_c + L_g) \dfrac{di_q}{dt} \right]}_{v_q'} - \omega_s (L_c + L_g) i_d \end{cases} \tag{8}$$

in which, those items v_d' and v_q' in brackets are utilized to design PI controllers for the d- and q-axis loops, and the other terms are treated as compensation items. The corresponding relationships of all the variables between d-q domain and the α-β domain are the following: i_g,$i_g^* \leftrightarrow i_d$,$i_q$, v_g,$v_g^* \leftrightarrow v_d$,$v_q$, v_{dc1}, and $v_{\mathrm{dc1}}^* \leftrightarrow v_{d1}$,$v_{q1}$. Fig. 4 illustrates the details of the d- and q-axis control loops for single-phase *LCL*-GCCs.

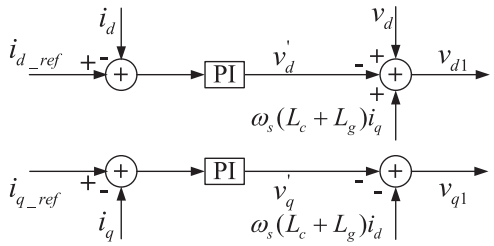

Fig. 4. Decoupled vector control for single-phase *LCL*-GCCs.

However, this simplification from *LCL*-GCCs to *L*-GCCs would result in imprecise description of the system and potential oscillatory and/or unstable dynamic behavior, if the *LCL* filter or the controller is not properly damped [6], [10].

III. Novel RNN-Based Vector Control

The proposed NN vector control architecture for a single-phase *LCL*-GCC is shown by Fig. 5. The controller has a nested-loop structure, consisting of a slow outer loop and a fast inner loop [25], [26]. The NN implements the fast inner current-loop control function. The outer control loops still utilize PI controllers. In the PCC voltage-oriented frame [10], the d-axis loop is used for active power or dc-link voltage control, and the q-axis loop is used for the reactive power or grid voltage support control as shown in Fig. 5. In Fig. 5, v_{d1}^* and v_{q1}^* are d- and q-axis voltages from the NN controller. $v_{\alpha 1}^*$ and $v_{\beta 1}^*$ are control voltage signals in α-β frame.

The proposed current-loop NN controller contains two parts: input preprocessing block and a four-layer feed-forward NN. To avoid input saturation, the inputs are regulated to the range $[-1, 1]$ through a preprocessing procedure. The inputs to the feed-forward NN are $\tanh(\overrightarrow{e_{\rm dq}}/Gain)$ and $\tanh(\overrightarrow{s_{\rm dq}}/Gain2)$, where $\overrightarrow{e_{\rm dq}}$ and $\overrightarrow{s_{\rm dq}}$ are error terms and integrals of the error terms. The calculation of $\overrightarrow{e_{\rm dq}}$ and $\overrightarrow{s_{\rm dq}}$ is the same as that for a general PI controller. The feed-forward NN contains two hidden layers of six nodes each, and two output nodes, with hyperbolic tangent functions at all nodes.

The NN current-loop controller can be denoted as $R(\overrightarrow{e_{\rm dq}}, \overrightarrow{s_{\rm dq}}, \overrightarrow{w})$, which is a function of $\overrightarrow{e_{\rm dq}}$, $\overrightarrow{s_{\rm dq}}$, and network weights $\overrightarrow{w}$. As the ratio of the converter output voltage $\overrightarrow{v_{\rm dq1}}$ to the outputs of the current loop controller $\overrightarrow{v_{\rm dq1}^*}$ is the gain of the pulse-width-modulation (PWM) which is denoted as $k_{\rm PWM}$ [24], the control action $\overrightarrow{v_{\rm dq1}}$ is then expressed by

$$\overrightarrow{v_{\rm dq1}} = k_{\rm PWM}\overrightarrow{v_{\rm dq1}^*} = k_{\rm PWM}R(\overrightarrow{e_{\rm dq}}, \overrightarrow{s_{\rm dq}}, \overrightarrow{w}) \tag{9}$$

Even though the feed-forward network in Fig. 6 does not have a feedback connection, the proposed NN controller shown in Fig. 5 actually is a recurrent neural network (RNN), because the feedback signal of the system acts as a recurrent network connection from the output of the NN and back to the input.The NN controller can be considered as a "super-PI" controller, which can be applied to an existing system without any other changes of system configuration or hardware interface.

IV. Training RNN Controller

A. State Space Model of LCL-GCC in d-q Frame

Equation (10) describes the system equation of an *LCL*-GCC [14], which will be used for NN training

$$\frac{d}{dt}\begin{bmatrix} i_d \\ i_q \\ i_{\rm dc\_d1} \\ i_{\rm dc\_q1} \\ v_{\rm cd} \\ v_{\rm cq} \end{bmatrix} = \begin{bmatrix} -\frac{R_g}{L_g} & \omega_s & 0 & 0 & -\frac{1}{L_g} & 0 \\ -\omega_s & -\frac{R_{g3}}{L_g} & 0 & 0 & 0 & -\frac{1}{L_g} \\ 0 & 0 & -\frac{R_c}{L_c} & \omega_s & \frac{1}{L_c} & 0 \\ 0 & 0 & -\omega_s & -\frac{R_c}{L_c} & 0 & \frac{1}{L_c} \\ \frac{1}{C} & 0 & -\frac{1}{C} & 0 & 0 & \omega_s \\ 0 & \frac{1}{C} & 0 & -\frac{1}{C} & -\omega_s & 0 \end{bmatrix} \begin{bmatrix} i_d \\ i_q \\ i_{\rm dc\_d1} \\ i_{\rm dc\_q1} \\ v_{\rm cd} \\ v_{\rm cq} \end{bmatrix} + \begin{bmatrix} \frac{1}{L_g} & 0 & 0 & 0 & 0 & 0 \\ 0 & \frac{1}{L_g} & 0 & 0 & 0 & 0 \\ 0 & 0 & -\frac{1}{L_c} & 0 & 0 & 0 \\ 0 & 0 & 0 & -\frac{1}{L_c} & 0 & 0 \\ 0 & 0 & 0 & 0 & 0 & 0 \\ 0 & 0 & 0 & 0 & 0 & 0 \end{bmatrix} \times \begin{bmatrix} v_d \\ v_q \\ v_{d1} \\ v_{q1} \\ 0 \\ 0 \end{bmatrix} \tag{10}$$

where ω_s is the angular frequency of the grid voltage, all other symbols are consistent with those shown in Fig. 1. The corresponding relationships of all the variables between d-q domain and the single-phase circuit domain are the following: i_g,i_g^* $\leftrightarrow$ i_d,i_q, $i_{\rm dc1}$,$i_{\rm dc1}^*$ $\leftrightarrow$ $i_{\rm dc\_d1}$,$i_{\rm dc\_q1}$, v_g,v_g^* $\leftrightarrow$ v_d,v_q, $v_{\rm dc1}$,$v_{\rm dc1}^*$ $\leftrightarrow$ v_{d1},v_{q1}, and v_c,v_c^* $\leftrightarrow$ $v_{\rm cd}$,$v_{\rm cq}$.

For implementation of the RNN-based digital controller as presented in Section III, the continuous state space model (10) needs to be transferred into the equivalent discrete model (11) through either a zero-order or first-order hold discrete equivalent mechanism [27]

$$\overrightarrow{i_{\rm dqs}}(k+1) = A\overrightarrow{i_{\rm dqs}}(k) + B\overrightarrow{u_{\rm dqs}}(k) \tag{11}$$

in which, $\overrightarrow{i_{\rm dqs}}$ and $\overrightarrow{u_{\rm dqs}}$ represent $[i_d, i_q, i_{d1}, i_{q1}, v_{\rm cd}, v_{\rm cq}]'$ and $[v_d, v_q, v_{d1}, v_{q1}, 0, 0]'$, respectively; A stands for system matrix and B is the input matrix.

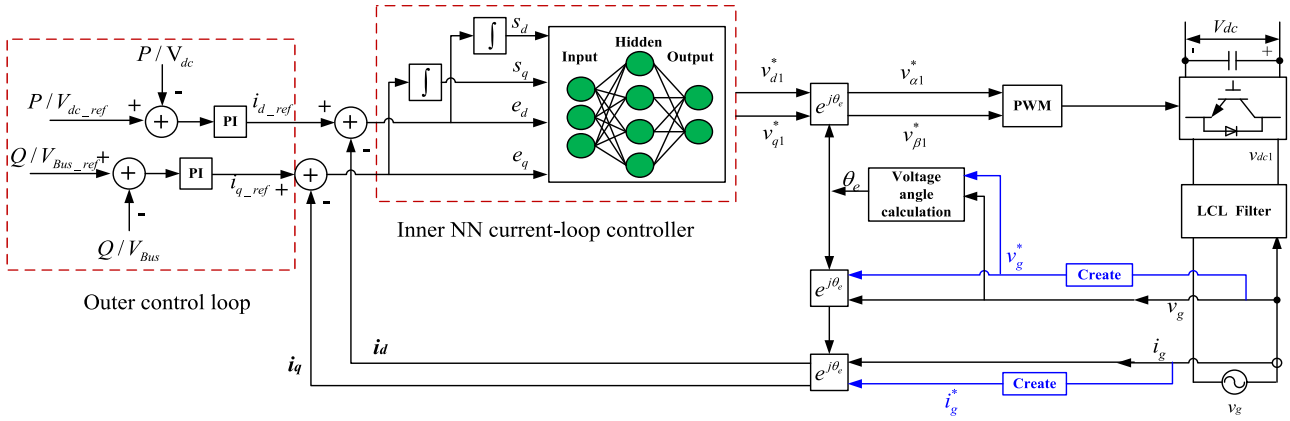

Fig. 5. RNN based vector control for single-phase *LCL*-GCCs.

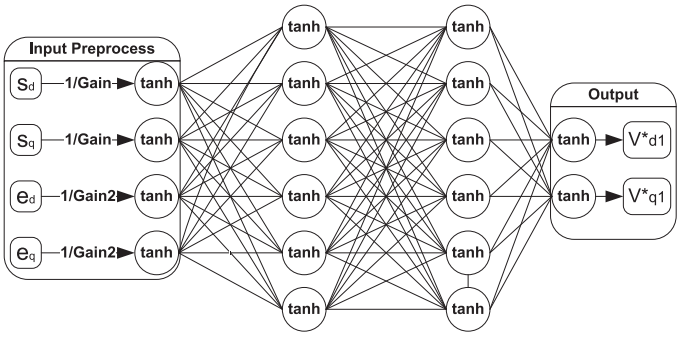

Fig. 6. RNN controller structure.

Note that in (10) and (11), v_{d1} and v_{q1} are control actions from current controller, while i_d and i_q are the grid currents that need to be controlled.

B. Training Objective: Approximate Optimal Control

Dynamic programming employs the principle of Bellman's optimality [17], and is a very useful tool for solving the optimization and optimal control problems. The typical structure of the discrete-time DP includes a discrete-time system model and a performance index or cost associated with the system [19].

The DP cost function associated with the *LCL*-GCC system is defined as

$$C_{\mathrm{dp}}=\sum_{k=j}^{\infty}\gamma^{k-j}U(\overrightarrow{e_{\mathrm{dq}}}(k)) =\sum_{k=j}^{\infty}\gamma^{k-j}\sqrt{[i_d(k)-i_{d\_\mathrm{ref}}(k)]^2+[i_q(k)-i_{q\_\mathrm{ref}}(k)]^2} \quad (12)$$

where j denotes the starting point and generally $j>0$, γ is a discount factor with $0<\gamma\leq 1$, and U is called local cost or utility function. The function C_{dp}, depending on the initial time j and the initial state $\overrightarrow{i_{\mathrm{dq}}}(j)$, is referred to as the cost-to-go of state $\overrightarrow{i_{\mathrm{dq}}}(j)$ of the DP problem. The objective of the training is to find an optimal trajectory of control action $\overrightarrow{v_{\mathrm{dq1}}}$ that minimizes the DP cost C_{dp} in (12). As the control action $\overrightarrow{v_{\mathrm{dq1}}}$ completely depends on the RNN current controller, the objective actually means finding the best NN weight $\overrightarrow{w}$ to approximate the optimal control.

C. RNN Training Algorithm: Levenberg–Marquardt + Forward Accumulation Through Time

We chose to use the LM algorithm to train an RNN because LM appears to be the fastest NN training algorithm for a moderate number of network parameters [28]. To implement LM training, the cost function defined in (12) needs to be rewritten in a sum-of-squares form. Consider the cost function C_{dp} with $\gamma=1$, $j=1$ and $k=1,\cdots,N$, then it can be written in the form

$$C_{\mathrm{dp}}=\sum_{k=1}^{N}U(\overrightarrow{e_{\mathrm{dq}}}(k)) \Longleftrightarrow^{\mathrm{def}\,V(k)=\sqrt{U(\overrightarrow{e_{\mathrm{dq}}}(k))}} C_{\mathrm{dp}}=\sum_{k=1}^{N}V^2(k) \quad (13)$$

and the gradient $\frac{\partial C_{\mathrm{dp}}}{\partial w}$ can be written in a matrix product form

$$\frac{\partial C_{\mathrm{dp}}}{\partial \overrightarrow{w}}=\sum_{k=1}^{N}V(k)\frac{\partial V(k)}{\partial \overrightarrow{w}}=2J_v(\overrightarrow{w})^TV \quad (14)$$

in which, the Jacobian matrix $J_v(\overrightarrow{w})$ is

$$J_v(w)=\begin{bmatrix}\frac{\partial V(1)}{\partial w_1} & \cdots & \frac{\partial V(1)}{\partial w_M}\\ \vdots & \ddots & \vdots \\ \frac{\partial V(N)}{\partial w_1} & \cdots & \frac{\partial V(N)}{\partial w_M}\end{bmatrix}, V=\begin{bmatrix}V(1)\\ \vdots \\ V(N)\end{bmatrix} \quad (15)$$

Therefore, the weights update by using LM [28]–[30] for an RNN controller can be expressed as

$$\triangle\overrightarrow{w}=-[J_v(\overrightarrow{w})^TJ_v(\overrightarrow{w})+\mu I]^{-1}J_v(\overrightarrow{w})^TV \quad (16)$$

In order to find Jacobian matrix $J_v(\overrightarrow{w})$, FATT is used in this paper for an *LCL*-GCC system, which incorporates the procedures of unrolling the system, calculating the derivatives of the

TABLE I
HARDWARE EXPERIMENT TEST SYSTEM PARAMETERS

Symbol	Quantity	Value	Unit
V_g	nominal grid voltage (rms)	120	V
f	nominal grid frequency	60	Hz
$V_{\rm dc}$	DC-link voltage	250	V
$C_{\rm dc}$	DC-link capacitance	3260	μF
L_c	*LCL*-filter converter-side inductor	12.5	mH
R_c	*LCL*-filter converter-side resistor	0.125	Ω
C	*LCL*-filter parallel capacitor	2.2	μF
R_{Cin}	*LCL*-filter capacitor internal resistance	3	Ω
L_g	*LCL*-filter grid-side inductor	12.5	mH
R_g	*LCL*-filter grid-side resistor	0.125	Ω

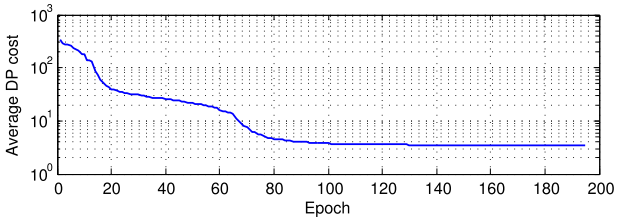

Fig. 7. Neural network controller learning curve.

Jacobian matrix, and calculating the DP cost into one single process for each training epoch [31], [32].

D. Training Implementation

Besides the LM+FATT algorithm shown in Section IV-C, we also used the following policies in the training:

1) l trajectories were used to train the RNN. l was generally chosen as 10;
2) the initial current state $\overrightarrow{i_{\rm dq}}(0)$ for each trajectory was generated randomly;
3) the d-q reference current for each trajectory was generated randomly and was changed every 0.1 s;
4) the initial weights $\overrightarrow{w}$ of the RNN were generated randomly;
5) the sampling time was chosen as $T_s = 1$ ms and the duration of each trajectory was set as 1 s.

The training of the NN controller could be also implemented considering the system parameter changes, e.g., the inductance can be varied for different trajectories or after a certain time period within each trajectory. The change of the inductance will cause the recalculation of the system (10) and (11). As a well-trained NN controller can tolerate a wide range of system parameter change (see [32]), this policy was not adopted in this paper.

Table I specifies the *LCL*-GCC system parameters.

Fig. 7 shows the learning curve for a successful training of the NN controller. The average DP cost per trajectory drops to a small value very quickly within 100 iterations and is stabilized at this value, demonstrating a good convergence result of the LM training algorithm.

V. PERFORMANCE EVALUATION

To evaluate the performance of the proposed NN vector controller and compare it with PR control and conventional

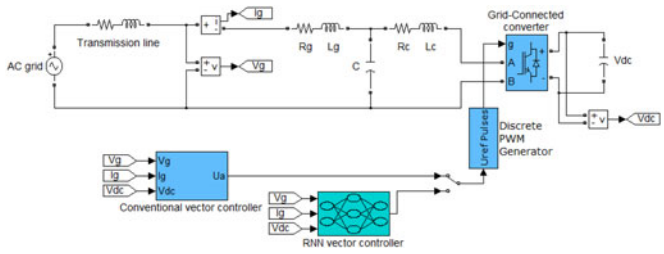

Fig. 8. Simulink model of a single-phase *LCL*-GCC using conventional decoupled vector control and novel NN vector control.

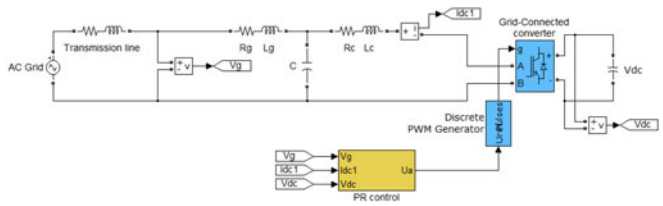

Fig. 9. Simulink model of a single-phase *LCL*-GCC using PR control.

vector control, integrated transient simulation systems of the single-phase *LCL*-GCC systems in the STATCOM applications were developed by using SimPowerSystems in Matlab. Fig. 8 shows the Simulink model of a single-phase *LCL*-GCC using conventional decoupled vector control and novel NN vector control.

The Simulink model of a single-phase *LCL*-GCC using PR control is demonstrated by Fig. 9. Note that in order to keep the direction of current the same as that in NN control and convention vector control, the direction of the measured inverter current is the opposite to that in Fig. 2, $e_i = i_{\rm dc1}\text{-}i_{\rm dc1\_ref}$. For PR control, the inverter current is measured in general, while for vector control, the grid current is sensed.

A. Controller Design

The PI parameters of the current-loop controller for the conventional vector control method was tuned by PID tuner function within the PID controller block in MATLAB. Phase margin was set as 60º and the bandwidth was chosen as 1500 rad/s, which tends to yield the best results considering the PWM saturation constraints. To overcome resonance phenomenon of the *LCL* filter, AD method was adopted in developing conventional vector control [33]. A low-pass filter is added to the output of the current-loop controller [34] at the resonance frequency [35]

$$f_r = \frac{1}{2\pi}\sqrt{\frac{L_g + L_c}{L_g L_c C}} \tag{17}$$

For the NN vector control, the NN current controller was trained using the LM+FATT algorithm described in Section IV. As the NN controller behaves naturally like a low-pass filter , no special damping policy is required to overcome the resonant problem [32].

The dc-link voltage control is developed based on the principle of the power balance [25] and the tuning for the dc-link voltage PI controller is similar to that for the current-loop controller. Phase margin was set as 60º. The bandwidth was chosen

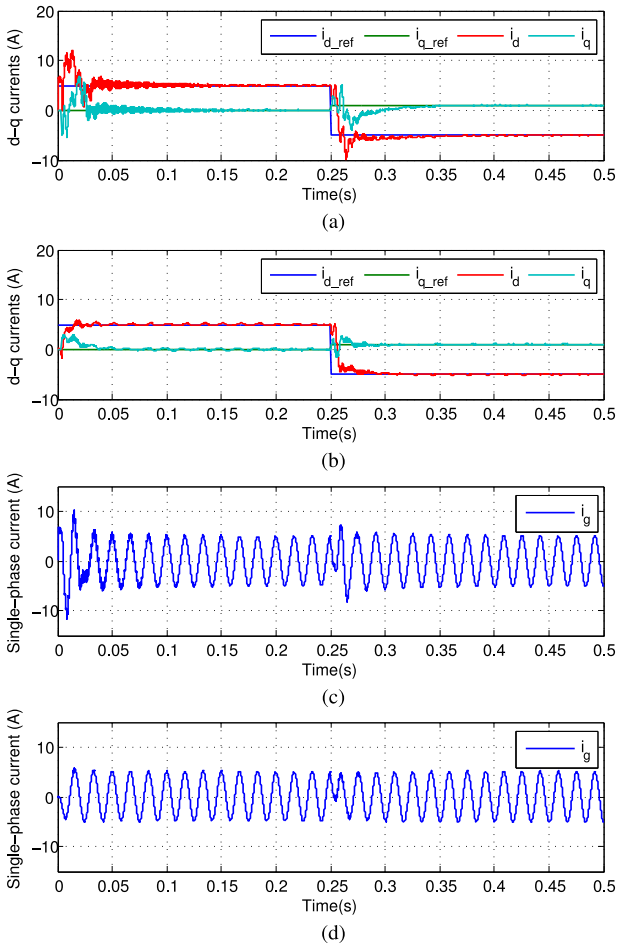

Fig. 10. Current tracking comparisons between conventional vector control and NN vector control. (a) Conventional vector control. (b) NN vector control. (c) Conventional vector control. (d) NN vector control.

as 4 rad/s because any bandwidth larger than 4 rad/s failed to maintain the dc-link voltage constant in all hardware experiments using the conventional vector control. To be fair for comparison, the bandwidth 4 rad/s was used also for the NN vector control.

For the PR control, the controller design followed the suggestions from [3], [15], [16]. Also, to be fair for comparison, the same PI parameters were used for the dc-link voltage control.

B. Performance Comparisons

If not specified, $T_s = 0.1$ ms was used in all simulations of Section V. Switching frequency $f_s = 3000$ Hz was used.

Fig. 10 compares the current tracking ability between conventional vector control and NN vector control. The NN controller [see Fig. 10(b)] provides faster response speed than the conventional vector controller [see Fig. 10(a)]. More importantly, the NN control shows smaller oscillations. Because the grid frequency $f = 60$ Hz, this causes the rounding error when determining how many cycles $(=\frac{1}{4fT_s})$ need to be delayed for generating the imaginary circuit. Thus, this rounding error caused the big oscillation using conventional vector control; however, the NN control can still provide acceptable

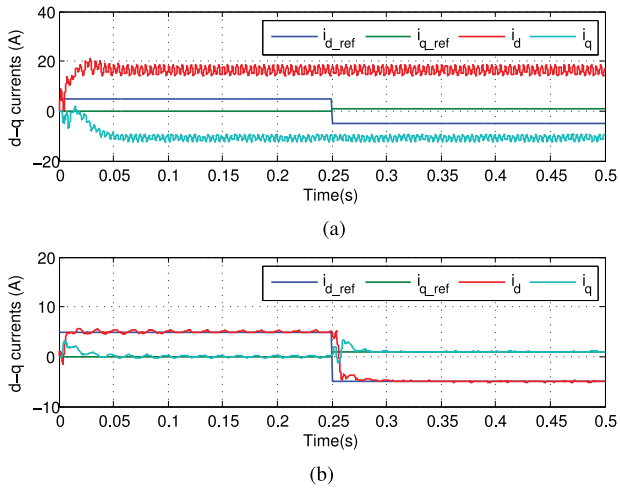

Fig. 11. Control performance comparisons between conventional vector control and NN vector control with implementation delays. (a) Conventional vector. (b) NN vector control.

performance. The single-phase current waveforms [see Figs. 10(c) and (d)] further demonstrates the good tracking performance of the NN controller.

Delays were added to the controller output to evaluate the NN controller performance further. Fig. 11 shows the performance between conventional vector control and NN vector control with $3T_s$ delays added. As the PR control does not have d-q currents, the comparison does not contain the results of the PR control. The NN control [see Fig. 11(b)] still performs well, while the conventional vector control [see Fig. 11(a)] has already lost the stability. In our tests, the NN control was significantly affected only until $9T_s$ delays were added to the controller output. In reality, this large delay is rare. Even though the delay is not considered in the design and training of the NN controller, the NN controller still performs well, demonstrating its robustness.

As the same parameters were used for the outer voltage loop PI controllers, the dc-link voltage tracking performance are exactly the same (12) for all three control methods.

For the inner current loop, the regulated current i_g are almost the same, however, the current under conventional vector control has slight oscillations [see Fig. 13(b)].

Compared to the conventional vector control, the NN vector control is a damping free technique, i.e., it does not need any special damping policies [see Fig. 13(c)]. Basically, all three control methods provide very good control performance in simulations; however whether they still can perform well in hardware experiments needs to be tested further.

VI. Hardware Experiment Validation

A. Experiment Setup

A hardware laboratory test system for a single-phase *LCL*-GCC in an STATCOM application was built to validate the proposed NN vector control method corresponding to the simulations [see Figs. 8 and 9].

The hardware test system took the following setups: 1) an ac/dc converter was connected to an adjustable LabVolt (see

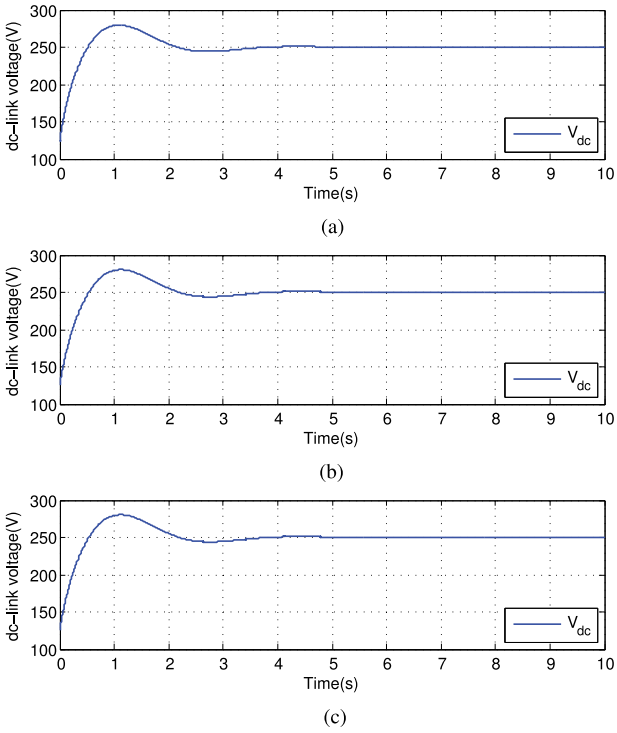

Fig. 12. Comparisons of dc-link voltage control. (a) PR control. (b) Conventional vector control. (c) NN vector control.

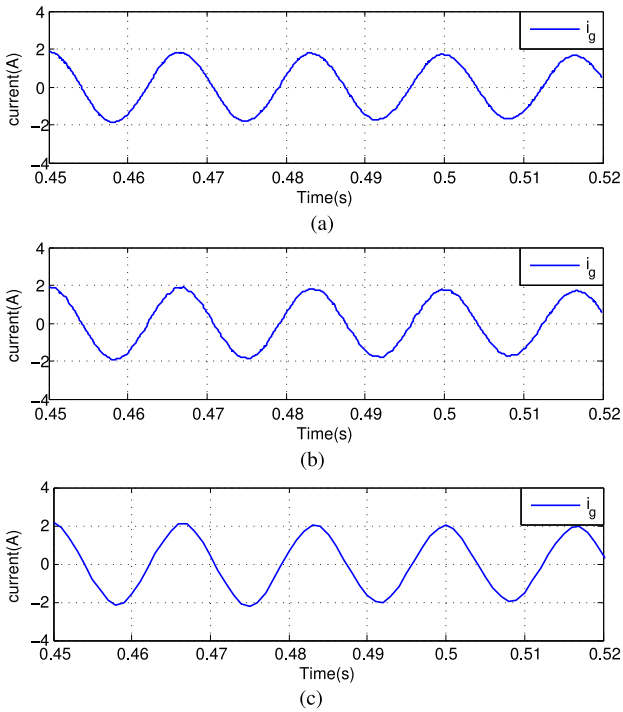

Fig. 13. Comparisons of grid current. (a) PR control. (b) Conventional vector control. (c) NN vector control.

[36]) single-phase power supply signifying the grid, 2) all filters were built by using LabVolt smoothing inductors and LabVolt capacitors, 3) the ac/dc converter was controlled by a dSPACE (see [37]) digital control system, 4) the control system collected the dc-link voltage and single-phase currents and voltages, and sends out control signals to the converter according to various control demands. Fig. 14 demonstrates an example of the hardware laboratory testing system.

To start the experiment, the power source representing the grid was first turned on and thus the dc-link capacitor was charged to around 167 V. Then, the controller was started from the control desk using the dSPACE. According to our laboratory experiment experience, a NN controller trained offline does not need to be retuned, while this is usually needed for a conventional controller.

B. Tracking Performance Comparison

Fig. 15 shows the grid voltage waveform in the laboratory and the grid voltage was distorted even before conducting the experiment.

We also found that the voltage source has an unexpected big internal inductance (around 50 mH). These uncertainties brought the challenges for all three control methods.

The sampling time $T_s = 0.1$ ms was used for the conventional vector control and the NN vector control. However, using sampling time $T_s = 0.1$ ms for PR control failed the experiment. The PR needs high sampling frequency, and it could succeed when using the sampling time $T_s = 0.02$ ms. Note that using even smaller sampling time $T_s = 0.01$ ms caused overrun problem

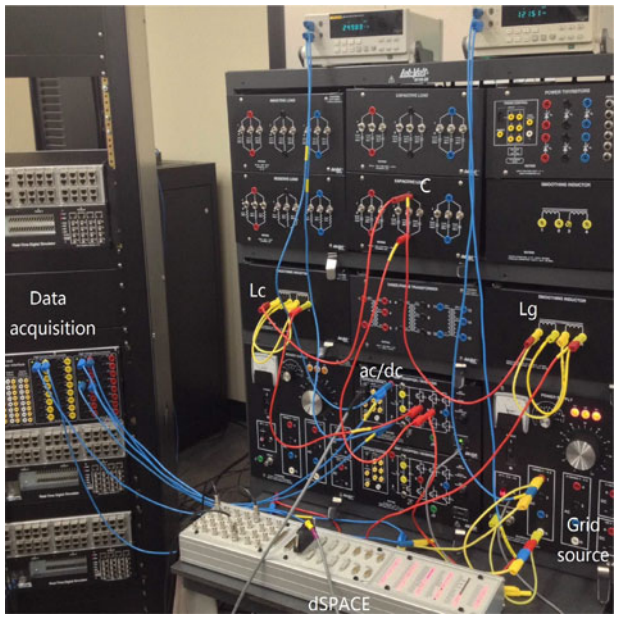

Fig. 14. Setup of hardware laboratory testing system.

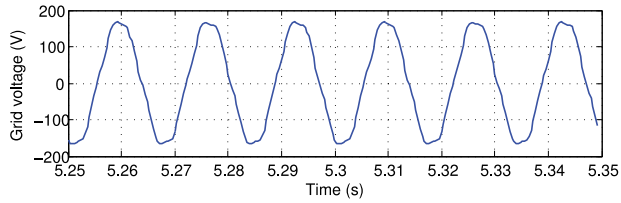

Fig. 15. Distorted grid voltage.

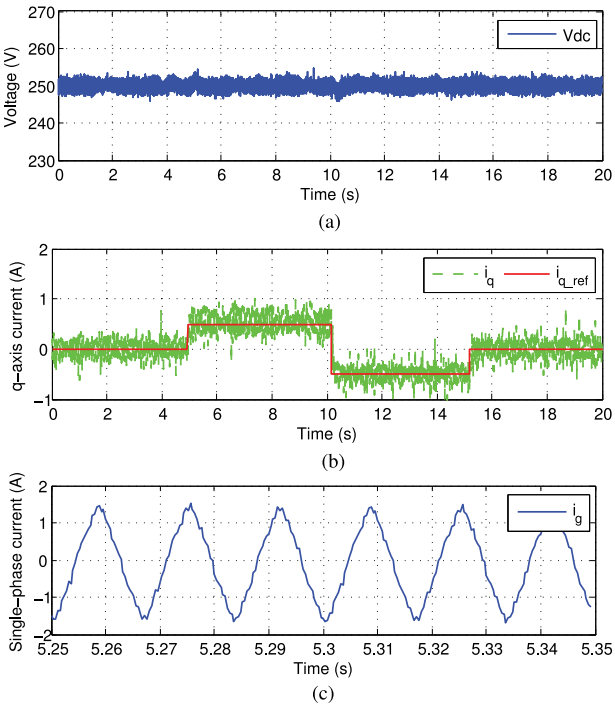

Fig. 16. NN vector control for single-phase *LCL*-GCC. (a) DC-link voltage. (b) PCC q-axis current waveform. (c) Single-phase current waveform.

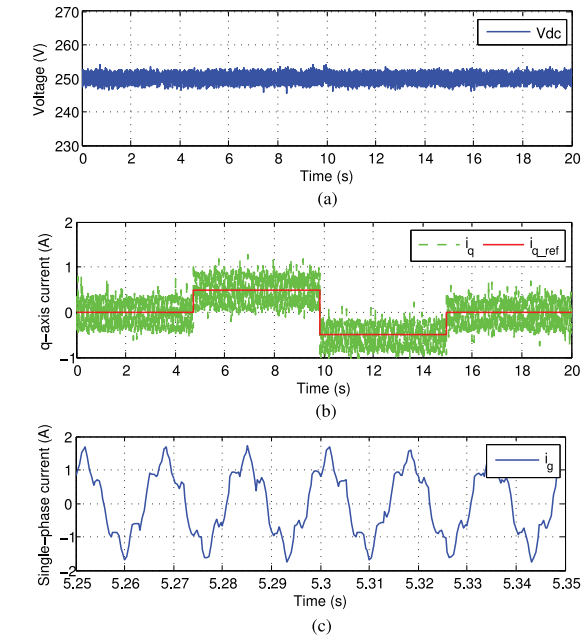

Fig. 17. Conventional vector control for single-phase LCL-GCC. (a) DC-link voltage. (b) PCC q-axis current waveform. (c) Single-phase current waveform.

using dSPACE. Thus, the sampling time $T_s = 0.02$ ms was used in all the experiments for the PR control.

Figs. 16–18 show the experiments for a single-phase *LCL*-GCC under novel NN vector control, conventional vector control, and PR control, respectively. The switching frequency f_s = 3000 Hz were used in the experiments. Both the NN vector control and conventional vector control could maintain the dc-link voltage more stable [see Figs. 16(a) and 17(a)] than the

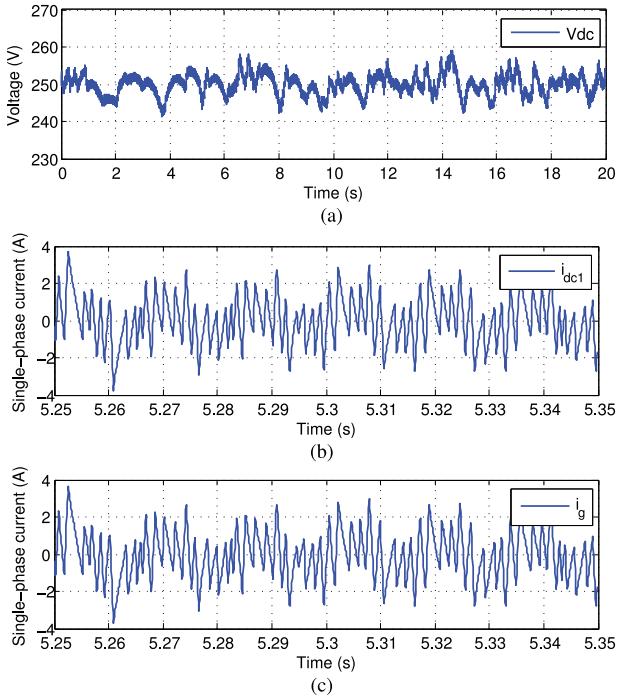

Fig. 18. PR control for single-phase LCL-GCC. (a) DC-link voltage. (b) single-phase current waveform. (c) single-phase current waveform.

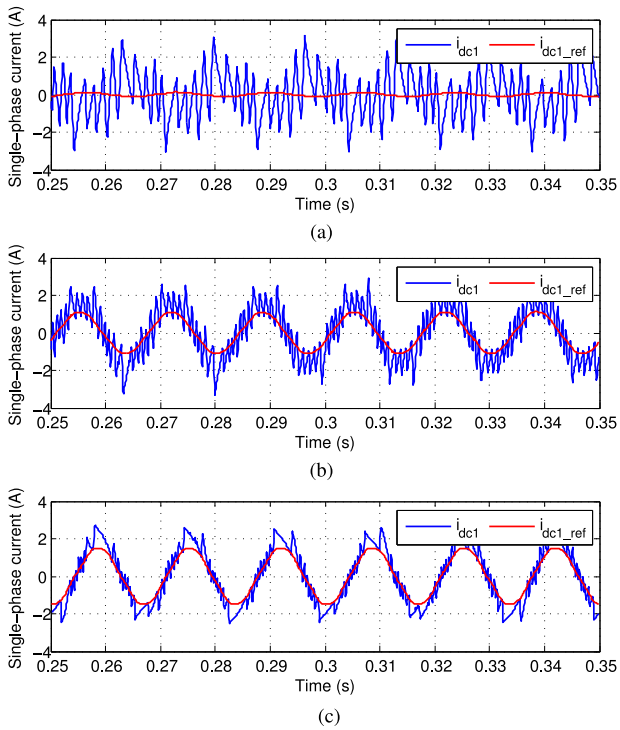

Fig. 19. Current tracking comparison using PR control with different switching frequencies. (a) 3000 Hz. (b) 6000 Hz. (c) 10 000 Hz.

PR control [see Fig. 18(a)]. Moreover, the current waveform demonstrated less oscillations under the NN vector control [see Figs. 16(b) and (c)] than that under the conventional vector control [see Fig. 17(b) and (c)]. Actually, the PR control [Fig. 18] performed much worse in the hardware experiment than in the

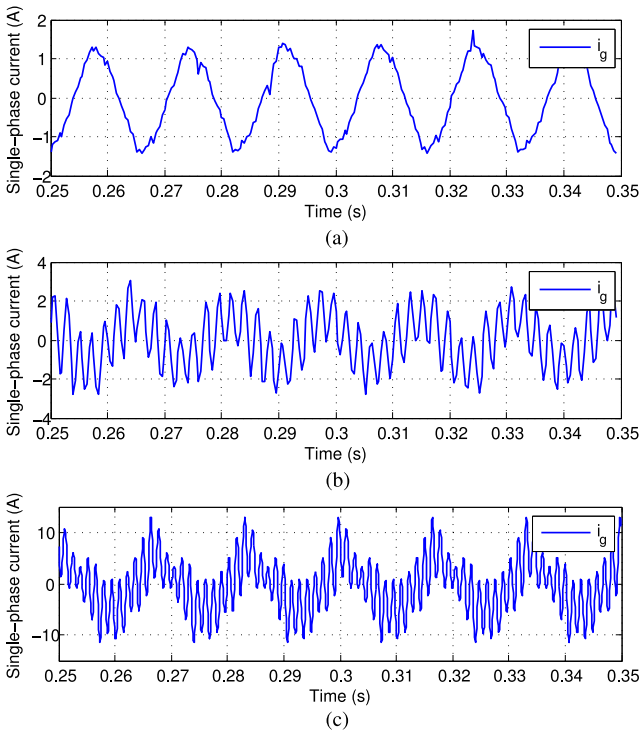

Fig. 20. Current waveform comparison with $C^* = 6.6\ \mu$F and $f_s = 3000$ Hz. (a) Single-phase current waveform using NN vector control. (b) Single-phase current waveform using conventional vector control. (c) Single-phase current waveform using PR control.

simulation (see Section V). The dc-link voltage see [Fig. 18(a)] was not stable and the currents had very large oscillations [see Fig. 18(b) and (c)].

To improve the performance of the PR control, a higher switching frequency needs to be used. Fig. 19 shows the comparison results for the PR control with different switching frequencies. When the switching frequency $f_s = 3000$ Hz, the current tracking performance [see Fig. 19(a)] was very poor. When the switching frequency was increased to $f_s = 6000$ Hz, the current tracking performance became better [see Fig. 19(b)]. Even better performance could be got when using the switching frequency $f_s = 10\ 000$ Hz [see Fig. 19(c)]. However, the high switching frequency generally causes more energy loss. Further, even using the switching frequency $f_s = 10000$ Hz, the PR control [Fig. 19(c)] still performed worse than both conventional and RNN vector control methods [Figs. 16(c) and 17(c)]. This seems to be consistent with the results shown in previously published articles [3], [15] in which the switching frequency used for a PR controlled converter is usually 10 kHz or higher.

C. Robustness Analysis

The RNN vector control method was further evaluated by considering system parameter changes. Fig. 20 shows the current waveforms under three control methods when the parallel capacitor was increased from 2.2 to 6.6 μF. The NN vector control still can perform very well, providing the similar results [see Fig. 20(a)] as that without the system parameter change [see Fig. 16(c)]. The conventional vector control had more oscillations [see Fig. 20(b)] due to the problem of the AD method, as it is more sensitive to system parameter change for AD method. The PR control yielded the worst performance [see Fig. 20(c)] among all three methods.

VII. Conclusion

This paper investigated a NN vector control method for a single-phase *LCL*-filter based GCC. The NN controller implements the optimal control based on the DP principle. Both the simulation evaluation and hardware experiment results demonstrated that the NN control technique has superior performance to the conventional control methods such as no requirement for damping policies, better performance facing system parameter change, and no need for high sampling and switching frequencies which is normally needed for the PR control. Using the NN vector control technique, the harmonics are significantly reduced due to better control performance, which would benefit the integration of small-scale single-phase renewable resources to the grid.

References

[1] O. S. Senturk, L. Helle, S. Munk-Nielsen, P. Rodriguez, and R. Teodorescu, "Power capability investigation based on electrothermal models of press-pack IGBT three-level NPC and ANPC VSCs for multimegawatt wind turbines," *IEEE Trans. Power Electron*, vol. 27, no. 7, pp. 3195–3206, Jul. 2012.

[2] W. Wu, Y. Sun, Z. Lin, T. Tang, F. Blaabjerg, and H. S. Chung, "A new LCL-filter with in-series parallel resonant circuit for single-phase grid-tied inverter," *IEEE Trans. Ind. Electron*, vol. 61, no. 9, pp. 4640–4644, Sep. 2014.

[3] S. B. Kjaer, J. K. Pedersen, and F. Blaabjerg, "Linear current control scheme with series resonant harmonic compensator for single-phase grid-connected photovoltaic inverters," *IEEE Trans. Ind. Electron.*, vol. 55, no. 7, pp. 1292–1306, Jul. 2008.

[4] X. Hao, X. Yang, T. Liu, L. Huang, and W. Chen, "A sliding-mode controller with multiresonant sliding surface for single-phase grid-connected VSI with an LCL filter," *IEEE Trans. Power Electron.*, vol. 28, no. 5, pp. 2259–2268, May 2013.

[5] M. Liserre, F. Blaabjerg, and S. Hansen, "Design and control of an LCL filter-based three-phase active rectifier," *IEEE Trans. Ind. Appl.*, vol. 41, no. 5, pp. 1281–1291, Oct. 2005.

[6] V. Blasko and V. Kaura, "A novel control to actively damp resonance in input LC filter of a three-phase voltage source converter," *IEEE Trans. Ind. Appl.*, vol. 33, no. 2, pp. 542–550, Mar./Apr. 1997.

[7] R. Zhang, M. Cardinal, P. Szczesny, and M. Dame, "A grid simulator with control of single-phase power converters in d-q rotating frame," in *Proc. IEEE 33rd Annu. Power Electron. Spec. Conf.*, Cairns, Qld., Australia, Jun. 2002, pp. 1431–1436.

[8] A. Roshan, R. Burgos, A. C. Baisden, F. Wang, and D. Boroyevich, "A D-Q frame controller for a full-bridge single phase inverter used in small distributed power generation systems," in *Proc. IEEE 22nd Annu. Conf. Appl. Power Electron*, Anaheim, CA, USA, Mar. 2007, pp. 641–647.

[9] B. Bahrani, A. Rufer, S. Kenzelmann, and L. A. C. Lopes, "Vector control of single-phase voltage-source converters based on fictive-axis emulation," *IEEE Trans. Ind. Appl.*, vol. 47, no. 2, pp. 831–840, Mar./Apr. 2011.

[10] J. Dannehl, C. Wessels, and F. W. Fuchs, "Limitations of voltage-oriented PI current control of grid-connected PWM rectifiers with *LCL* filters," *IEEE Trans. Ind. Electron.*, vol. 56, no. 2, pp. 380–388, Feb. 2009.

[11] W. Wu, Y. Sun, M. Huang, X. Wang, H. Wang, F. Blaabjerg, M. Liserre, and H. S. Hung Chung, "A robust passive damping method for *LLCL*-filter-based grid-tied inverters to minimize the effect of grid harmonic voltages," *IEEE Trans. Power Electron.*, vol. 29, no. 7, pp. 3279–3289, Jul. 2014.

[12] C. Bao, X. Ruan, X. Wang, W. Li, D. Pan, and K. Weng, "Step-by-step controller design for *LCL*-type grid-connected inverter with capactior-current-feedback active-damping," *IEEE Trans. Power Electron.*, vol. 29, no. 3, pp. 1239–1253, Mar. 2014.

[13] D. Pan, X. Ruan, C. Bao, W. Li, and X. Wang, "Capacitor-current-feedback active damping with reduced computation delay for improving robustness of *LCL*-type grid-connected inverter," *IEEE Trans. Power Electron.*, vol. 29, no. 7, pp. 3414–3427, Jul. 2014.
[14] R. Teodorescu, M. Liserre, and P. Rodriguez, *Grid Converters for Photovoltaic and Wind Power Systems*. Chichester, West Sussex, U.K.: Wiley, 2011.
[15] N. Zhang, H. Tang, and C. Yao, "A systematic method for designing a PR controller and active damping of the *LCL* filter for single-phase grid-connected PV inverters," *Energies*, vol. 7, no. 6, pp. 3934–3954, Jun. 2014.
[16] A. G. Yepes, F. D. Freijedo, and J. Doval-Gandoy, "On the discrete-time implementation of resonant controllers for active power filters," in *Proc. 35th Annu. Conf. IEEE Ind. Electron.*, Porto, Portugal, Nov. 2009, pp. 3686–3691.
[17] R. E. Bellman, *Dynamic Programming*. Princeton, NJ, USA: Princeton Univ. Press, 1957.
[18] S. N. Balakrishnan and V. Biega, "Adaptive-critic-based neural networks for aircraft optimal control," *J. Guidance, Control Dynam.*, vol. 19, no. 4, pp. 893–898, Jul./Aug. 1996.
[19] D. V. Prokhorov and D. C. Wunsch, "Adaptive critic designs," *IEEE Trans. Neural Netw.*, vol. 8, no. 5, pp. 997–1007, Sep. 1997.
[20] F. Wang, H. Zhang, and D. Liu, "Adaptive dynamic programming: An introduction," *IEEE Comput. Intell. Mag.*, vol. 4, no. 2, pp. 39–47, May 2009.
[21] G. K. Venayagamoorthy, R. G. Harley, and D. C. Wunsch, "Comparison of heuristic dynamic programming and dual heuristic programming adaptive critics for neurocontrol of a turbogenerator," *IEEE Trans. Neural Netw.*, vol. 13, no. 3, pp. 764–773, May 2002.
[22] S. Li, M. Fairbank, D. C. Wunsch, and E. Alonso, "Vector control of a grid-connected rectifier/inverter using an artificial neural network," in *Proc. IEEE World Congr. Comput. Intell.*, Brisbane, Qld., Australia, Jun. 2012, pp. 1–7.
[23] S. Li, M. Fairbank, C. Johnson, D. C. Wunsch, E. Alonso, and J. L. Proaño, "Artificial neural networks for control of a grid-connected rectifier/inverter under disturbance, dynamic and power converter switching conditions," *IEEE Trans. Neural Netw. Learn. Syst*, vol. 25, no. 4, pp. 738–750, Apr. 2014.
[24] N. Mohan, T. M. Undeland, and W. P. Robbins, *Power Electronics: Converters, Applications, and Design*, 3rd ed. Chichester, West Sussex, U.K.: Wiley, 2002.
[25] S. Li, T. A. Haskew, Y.-K. Hong, and L. Xu, "Direct-current vector control of three-phase grid-connected rectifier–inverter," *Electr. Power Syst. Res.*, vol. 81, no. 2, pp. 357–366, Feb. 2011.
[26] J. Rocabert, G. M. S. Azevedo, A. Luna, J. M. Guerrero, J. I. Candela, and P. Rodriguez, "Intelligent connection agent for three-phase grid-connected microgrids," *IEEE Trans. Power Electron.*, vol. 26, no. 10, pp. 2993–3005, Oct. 2011.
[27] G. F. Franklin, J. D. Powell, and M. L. Workman, *Digital Control of Dynamic Systems*. Reading, MA, USA: Addison-Wesley, 1998.
[28] M. T. Hagan and M. B. Menhaj, "Training feedforward networks with the Marquardt algorithm," *IEEE Trans. Neural Netw.*, vol. 5, no. 6, pp. 989–993, Nov. 1994.
[29] K. Levenberg, "A method for the solution of certain non-linear problems in least squares," *Quart. J. Appl. Math.*, vol. II, no. 2, pp. 164–168, 1994.
[30] D. W. Marquardt, "An algorithm for least-squares estimation of nonlinear parameters," *J. Soc. Ind. Appl. Math.*, vol. 11, no. 2, pp. 431–441, Jun. 1963.
[31] X. Fu, S. Li, M. Fairbank, D. C. Wunsch, and E. Alonso, "Training recurrent neural networks with the Levenberg–Marquardt algorithm for optimal control of a grid-connected converter," *IEEE Trans. Neural Netw. Learn. Syst.*, vol. 26, no. 9, pp. 1900–1912, Sep. 2015.
[32] X. Fu, S. Li, and I. Jaithwa, "Implement optimal vector control for *LCL*-filter-based grid-connected converters by using recurrent neural networks," *IEEE Trans. Ind. Electron.*, vol. 62, no. 7, pp. 4443–4454, Jul. 2015.
[33] R. Peña-Alzola, M. Liserre, F. Blaabjerg, R. Sebastián, J. Dannehl, and F. W. Fuchs, "Analysis of the passive damping losses in *LCL*-filter-based grid converters," *IEEE Trans. Power Electron.*, vol. 28, no. 6, pp. 2642–2646, Jun. 2013.
[34] J. Dannehl, M. Liserre, and F. W. Fuchs, "Filter-based active damping of voltage source converters with *LCL* filter," *IEEE Trans. Ind. Electron.*, vol. 58, no. 8, pp. 3623–3633, Aug. 2011.
[35] K. Jalili and S. Bernet, "Design of *LCL* filters of active-front-end two level voltage-source converters," *IEEE Trans. Ind. Electron.*, vol. 56, no. 5, pp. 1674–1689, May 2009.
[36] Festo didactic inc., [Online]. Available: https://www.labvolt.com/
[37] dSPACE Inc., [Online]. Available: http://www.dspace.com/

Xingang Fu (S'14) received the B.S. and M.S. degrees in applied mathematics from the Ocean University of China, Qingdao, China, in 2005 and 2009, respectively. He is currently working towards the Ph.D. degree with the Electrical and Computer Engineering Department, University of Alabama, Tuscaloosa, AL, USA.

His main research interests include neural network control, machine learning, cloud computing, data mining, power systems, and electric machines and drives.

Shuhui Li (S'99–M'99–SM'08) received the B.S. and M.S. degrees in electrical engineering from Southwest Jiaotong University, Chengdu, China, in 1983 and 1988, respectively, and the Ph.D. degree in electrical engineering from Texas Tech University, Lubbock, TX, USA, in 1999.

From 1988 to 1995, he was with the School of Electrical Engineering, Southwest Jiaotong University,, where his research interests included electrified railways, power electronics, power systems, and power system harmonics. From 1995 to 1999, he was involved in research on wind power, artificial neural networks, and applications of massive parallel processing. He joined Texas A&M University, Kingsville, TX, USA, in 1999, and an Associate Professor in 2003. He joined the University of Alabama, Tuscaloosa, AL, USA, as an Associate Professor, in 2006. His current research interests include renewable energy systems, power electronics, power systems, electric machines and drives, and applications of artificial neural networks in energy systems.